A Rab11a-Rab8a-Myo5B network promotes stretch-regulated exocytosis in bladder umbrella cells

Puneet Khandelwal[a], H. Sandeep Prakasam[a], Dennis R. Clayton[a], Wily G. Ruiz[a], Luciana I. Gallo[a], Daniel van Roekel[a], Stefan Lukianov[a], Johan Peränen[b], James R. Goldenring[c], and Gerard Apodaca[a,d]

[a]Departments of Medicine and [d]Cell Biology, University of Pittsburgh, Pittsburgh, PA 15261; [b]Institute of Biotechnology, University of Helsinki, 00014 Helsinki, Finland; [c]Department of Surgery and Epithelial Biology Center, Vanderbilt University, Nashville, TN 37232

ABSTRACT **Multiple Rabs are associated with secretory granules/vesicles, but how these GTPases are coordinated to promote regulated exocytosis is not well understood. In bladder umbrella cells a subapical pool of discoidal/fusiform-shaped vesicles (DFVs) undergoes Rab11a-dependent regulated exocytosis in response to bladder filling. We show that Rab11a-associated vesicles are enmeshed in an apical cytokeratin meshwork and that Rab11a likely acts upstream of Rab8a to promote exocytosis. Surprisingly, expression of Rabin8, a previously described Rab11a effector and guanine nucleotide exchange factor for Rab8, stimulates stretch-induced exocytosis in a manner that is independent of its catalytic activity. Additional studies demonstrate that the unconventional motor protein myosin5B motor (Myo5B) works in association with the Rab8a–Rab11a module to promote exocytosis, possibly by ensuring transit of DFVs through a subapical, cortical actin cytoskeleton before fusion. Our results indicate that Rab11a, Rab8a, and Myo5B function as part of a network to promote stretch-induced exocytosis, and we predict that similarly organized Rab networks will be common to other regulated secretory pathways.**

Monitoring Editor
Keith E. Mostov
University of California, San Francisco

Received: Aug 2, 2012
Revised: Jan 29, 2013
Accepted: Jan 30, 2013

INTRODUCTION

Rabs are a large family of small GTPases (44 subfamilies in humans) that regulate multiple steps in membrane traffic, including the uncoating, movement, maturation, tethering, and fusion of vesicles with their target membranes (Diekmann *et al.*, 2011; Hutagalung and Novick, 2011). Of the Rabs identified, Rab3 (a–d isoforms), Rab26, Rab27 (a and b isoforms), and Rab37 are referred to as "secretory" Rabs because of their association in neuroendocrine cells with regulated secretion (Fukuda, 2008); that is, those pathways in which a storage pool of secretory vesicles/granules fuses with the plasma membrane in response to extracellular stimuli. The role of other "nonsecretory" Rabs in regulated secretion is not well understood or documented, despite the association of many of these Rabs with purified secretory granules (Brunner *et al.*, 2007; Casey *et al.*, 2007; Rindler *et al.*, 2007) and observations that they can promote regulated secretion in different cell types (Duman *et al.*, 1999; Khvotchev *et al.*, 2003). Furthermore, regulated secretory pathways often depend on multiple Rabs (Fukuda, 2008; Pavlos and Jahn, 2011), but the hierarchy of these Rabs and their relationships to one another remain to be defined.

In bladder umbrella cells, Rab11a, a well-known regulator of endocytic recycling in other cell systems (Ullrich *et al.*, 1996; Casanova *et al.*, 1999; Lapierre *et al.*, 2001; Knodler *et al.*, 2010), is associated with an abundant subapical pool of discoidal/fusiform-shaped vesicles (DFVs), which are enriched in the apical membrane protein uroplakin 3a (UP3a; Khandelwal *et al.*, 2008; Hudoklin *et al.*, 2012), one of four major UP species that make up the asymmetric unit membrane of the umbrella cell (Wu *et al.*, 2009). DFVs are distinct from

This article was published online ahead of print in MBoC in Press (http://www.molbiolcell.org/cgi/doi/10.1091/mbc.E12-08-0568) on February 6, 2013.

Address correspondence to: Gerard Apodaca (gla6@pitt.edu).

Abbreviations used: DFV, discoidal/fusiform-shaped vesicle; GAP, GTPase-activating protein; GEF, guanine nucleotide exchange factor; Myo5B, myosin5B motor; UP, uroplakin.

the endocytic system and instead form de novo from the *trans*-Golgi network (TGN; Khandelwal *et al.*, 2008, 2010; Hudoklin *et al.*, 2009). On exit from this compartment, DFVs mature and move toward the subapical region of the cell, where they are enmeshed in a cytokeratin network (Veranic and Jezernik, 2002; Guo *et al.*, 2009; Hudoklin *et al.*, 2012). In response to increased apical membrane tension (i.e., as a result of bladder filling) and an attendant rise in Ca^{2+}, they undergo an actin- and Rab11a-dependent exocytosis, dramatically increasing apical plasma membrane surface area (Lewis and de Moura, 1982; Wang *et al.*, 2003; Khandelwal *et al.*, 2008; Yu *et al.*, 2009). The proteins that are modulated by and act downstream of Rab11a to promote stretch-induced DFV exocytosis are unknown, although the cytoskeletal motor protein myosin 5B (Myo5B) is a known Rab11a effector, as well as Rab8a and Rab10 effector, in other cellular events (Lapierre *et al.*, 2001; Volpicelli *et al.*, 2002; Wakabayashi *et al.*, 2005; Varthakavi *et al.*, 2006; Nedvetsky *et al.*, 2007; Swiatecka-Urban *et al.*, 2007; Provance *et al.*, 2008; Chu *et al.*, 2009; Roland *et al.*, 2011; Schuh, 2011; Xu *et al.*, 2011).

To better understand the dependence of DFV exocytosis on Rab11a, we turned to an analogous, albeit constitutive secretory pathway that has been carefully dissected in the budding yeast *Saccharomyces cerevisiae*. In this organism, newly synthesized secretory vesicles emerge from the late Golgi under the control of Ypt31p/32p, paralogues of Rab11 (Benli *et al.*, 1996). GTP-bound Ypt31p/32p recruits Sec2p, a guanine nucleotide exchange factor (GEF) for Sec4p. The Sec4p GTPase is homologous to Rab8 and associates with vesicles before their fusion with the emerging bud (Ortiz *et al.*, 2002). An important effector in this system is Myo2p, a Myo5-like protein that interacts with both Ypt31p/32p and Sec4p and is responsible for actin-dependent delivery of the vesicles from the Golgi to the plasma membrane (Lipatova *et al.*, 2008; Jin *et al.*, 2011). Furthermore, Myo2p associates with Sec15p, a component of the octameric exocyst complex that tethers secretory vesicles to the plasma membrane before fusion (Jin *et al.*, 2011). Sec15p also serves as an effector of Sec4p (Jin *et al.*, 2011), and by its reported binding to Sec2p it may aid in the recruitment of Sec4p (Medkova *et al.*, 2006). We now show that an evolutionarily conserved Rab11a–Rab8a module along with Myo5B functions in umbrella cells to modulate stretch-induced DFV exocytosis.

RESULTS

DFV exocytosis is dependent on the Myo5B motor protein

We previously identified Rab11a as a modulator of DFV exocytosis (Khandelwal *et al.*, 2008), and hence our initial goal was to identify molecules that acted downstream of this GTPase to promote DFV fusion. A well-known effector of Rab11a is the Myo5 motor protein, which promotes long-range as well as local actin-based movements (Lapierre *et al.*, 2001; Volpicelli *et al.*, 2002; Wakabayashi *et al.*, 2005; Varthakavi *et al.*, 2006; Nedvetsky *et al.*, 2007; Swiatecka-Urban *et al.*, 2007; Provance *et al.*, 2008; Chu *et al.*, 2009; Roland *et al.*, 2011; Schuh, 2011; Xu *et al.*, 2011). Despite the actin dependence of apical exocytosis and apical endocytosis in umbrella cells (Lewis and de Moura, 1982; Yu *et al.*, 2009; Khandelwal *et al.*, 2010), a cortical actin cytoskeleton is reported to be absent from the apical pole of the umbrella cell (Romih *et al.*, 1999; Wang *et al.*, 2008). In our studies we observed that the amount of actin staining is variable at this surface (Acharya *et al.*, 2004), prompting us to explore different fixation protocols. We found that a critical factor was fixation at 37°C, and at this temperature a meshwork of actin was found at the apical surface (Figure 1A). The cortical actin cytoskeleton was more apical than, and distinct from, an apical meshwork of cytokeratins, which was previously shown to encase clusters of DFVs (Figure 1A; Veranic and Jezernik, 2002). Thus an actin-based motor is likely to be required at late steps in the exocytic pathway, after DFV movement through the cytokeratin network and before access to the apical plasma membrane.

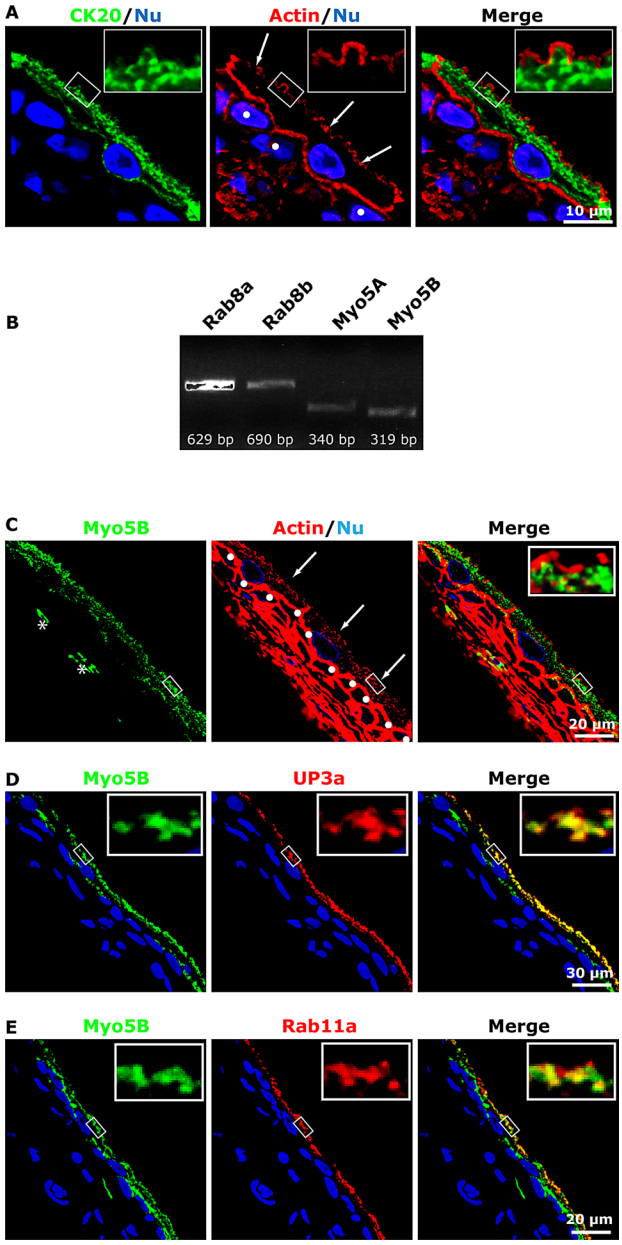

FIGURE 1: Presence of a subapical actin cytoskeleton in umbrella cells and expression of Myo5B in rat uroepithelium. (A) Distribution of cytokeratin 20 (CK20), the phalloidin-labeled actin cytoskeleton, and ToPro3-labeled nuclei (Nu) in cross-sectioned uroepithelium. Middle, arrows indicate the position of the umbrella cell apical membrane, and intermediate cells are marked with filled circles. (B) RT-PCR detection of Rab8a, Rab8b, Myo5A, and Myo5B message in rat uroepithelium. (C) Distribution of endogenous Myo5B in uroepithelium. Arrows point to the apical surface of the umbrella cell layer, and the first layer of intermediate cells is marked with filled circles. Right, inset, a magnified view of the boxed region in the parent image file. In some sections, Myo5B expression was also detected in cells within the lamina propria, examples of which are marked with an asterisk. (D, E) Colocalization of Myo5B with UP3a (D) or Rab11a (E). The epithelium in D and E more stretched than that in C.

Marker	M_X colocalization coefficient	M_Y colocalization coefficient
Myo5B (X) + UP3a (Y)	0.70 ± 0.02	0.74 ± 0.02
Myo5B (X) + Rab11a (Y)	0.52 ± 0.02	0.50 ± 0.02
Myo5B-tail (X) + Rab11a (Y)	0.84 ± 0.01	0.76 ± 0.01
Myo5B-tail (X) + UP3a (Y)	0.96 ± 0.01	0.84 ± 0.01
Myo5B-tail (X) + TGN-38 (Y)	0.21 ± 0.02	0.40 ± 0.06
Myo5B-tail (X) and Rab8 (Y)	0.04 ± 0.01	0.23 ± 0.07
Myo5B-tail (X) and Rabin8 (Y)	0.06 ± 0.03	0.38 ± 0.14
Rab11a (X) + Rab8 (Y)	0.57 ± 0.02	0.43 ± 0.03
AUM (X) + Rab8 (Y)	0.54 ± 0.02	0.53 ± 0.03
Rab8 (X) + Rabin8 (Y)	0.70 ± 0.02	0.75 ± 0.02
Rab11 (X) + Rabin8 (Y)	0.64 ± 0.06	0.89 ± 0.07
Myo5b (X) and nuclei (Y)	0.07 ± 0.02	0.05 ± 0.01

As a negative control we performed colocalization of Myo5B and nuclei, which showed only a limited degree of colocalization. Data are mean ± SEM; $n \geq 6$ random sections. AUM, asymmetric unit membrane.

TABLE 1: Manders' colocalization coefficients M_X and M_Y for the indicated pair of markers.

Both Myo5A and Myo5B mRNA expression were detected in the uroepithelium (Figure 1B). Because Myo5B is a well-known effector of Rab11a (Lapierre *et al.*, 2001; Volpicelli *et al.*, 2002; Wakabayashi *et al.*, 2005; Varthakavi *et al.*, 2006; Nedvetsky *et al.*, 2007; Swiatecka-Urban *et al.*, 2007; Provance *et al.*, 2008; Chu *et al.*, 2009; Roland *et al.*, 2011; Schuh, 2011; Xu *et al.*, 2011), we focused on this isoform. Its expression was confirmed by immunofluorescence analysis, which showed that endogenous Myo5B localized to punctate vesicular elements, reminiscent of DFV, just underneath the apical domain of the umbrella cells. Myo5B was also observed in the upper cytoplasm of the first layer of intermediate cells (Figure 1C), which also have DFVs (Apodaca, 2004), and in cells in the underlying lamina propria (examples are marked with an asterisk in Figure 1C). The association of Myo5B with DFV was confirmed by showing that Myo5B colocalized with the DFV cargo molecule UP3a (Figure 1D; see Table 1 for colocalization coefficients). Myo5B also colocalized, but to a somewhat lesser extent, with the DFV marker protein Rab11a (Figure 1E and Table 1).

As further evidence of an interaction between Myo5B and DFV, we transduced umbrella cells in situ using an adenovirus expressing the C-terminal cargo-binding domain of Myo5B fused to green fluorescent protein (GFP; Myo5B-tail; Lapierre *et al.*, 2001). In situ transduction primarily targets the umbrella cell layer (Khandelwal *et al.*, 2008), and in the present experiments the transduction efficiency was >80%. When expressed exogenously, the cargo-binding domains of myosin motors generate a dominant-negative phenotype that is marked by clustering of the motor and its select cargoes within the cell cytoplasm (Lapierre *et al.*, 2001; Volpicelli *et al.*, 2002; Wakabayashi *et al.*, 2005; Chu *et al.*, 2009; Roland *et al.*, 2011; Xu *et al.*, 2011). These characteristics were apparent when the size and distribution of endogenous UP3a, Rab11a, and TGN-38 in umbrella cells were compared with cells expressing GFP-tagged Myo5B-tail (compare Figure 2A to Figure 2, B–D). The transduced samples contained large, vesicular-appearing, Myo5B-tail-positive clusters that showed extensive colocalization with UP3a or Rab11a (Table 1). In contrast to Rab11a and UP3a, the non-Myo5B cargo protein TGN-38 showed significantly less colocalization with the Myo5B-tail ($p < 0.5$; Figure 2D and Table 1). Furthermore, when cross sections of GFP- (control) or GFP-Myo5B–expressing cells were examined by transmission electron microscopy, only the latter showed clusters of DFVs, which appeared smaller than vesicles observed in control cells (Figure 2E). Stacks of Golgi appeared in proximity to, but distinct from, the clustered DFVs when cells were examined by electron microscopy (Figure 2E).

To determine whether Myo5B modulated stretch-induced exocytosis, we transduced umbrella cells with GFP- (control) or Myo5B-tail–encoding adenoviruses and exposed the isolated bladders to experimental filling (i.e., stretch). As a measure of exocytosis, we monitored changes in capacitance (C_T; where 1 μF ≈ 1 cm^2 of surface area), which increase in response to stretch and show good concordance with other measures of exocytosis (Truschel *et al.*, 2002; Khandelwal *et al.*, 2008; Yu *et al.*, 2009). Myo5B-tail caused a significant decrease in stretch-induced changes in C_T compared with control tissues (Figure 3A). The importance of Myo5B was also shown by experiments in which umbrella cells were transduced with both Myo5B-tail and human growth hormone, which is packaged into DFV and secreted in response to bladder filling (Kerr *et al.*, 1998; Khandelwal *et al.*, 2008). In these studies, Myo5B-tail caused a significant ~70% decrease in growth hormone release after 2 h of filling the bladders (Figure 3B).

Rab8a acts with Rab11a to regulate DFV exocytosis

Our next goal was to examine whether Rab11a worked in conjunction with Rab8 to promote DFV exocytosis. Reverse transcription (RT)-PCR confirmed the expression of Rab8a/b in the uroepithelium (Figure 1B). Because we could not find an Rab8a- or Rab8b-selective antibody for use in our studies, we used an antibody that recognizes both isoforms of this GTPase. Thus, when describing the localization of Rab8, we do not make a distinction between its two isoforms. Rab8 was associated with punctate vesicular structures at the apical pole of the cell that colocalized with UPs (Figure 4, A and B, and Table 1). We also observed Rab8-positive vesicles that were localized in the bottom half of the umbrella cell (Figures 4A and 5F). These likely represent Rab8-positive vesicular intermediates involved in other trafficking events such as transport of newly synthesized proteins to the basolateral cell surface (Huber *et al.*, 1993). When umbrella cells were transduced with the GFP-tagged, dominant-negative mutant Rab8aT_{22}N (DN-Rab8a), there was a significant decrease in stretch-induced changes in C_T (Figure 4C). We previously reported that changes in C_T were not observed in quiescent tissues not exposed to stretch (Truschel *et al.*, 2002). However, expression of dominant-active RFP-tagged Rab8a-Q_{67}L (DA-Rab8a) caused a significant increase in C_T above stretched or unstretched control tissues (Figure 4D). This last phenotype was similarly

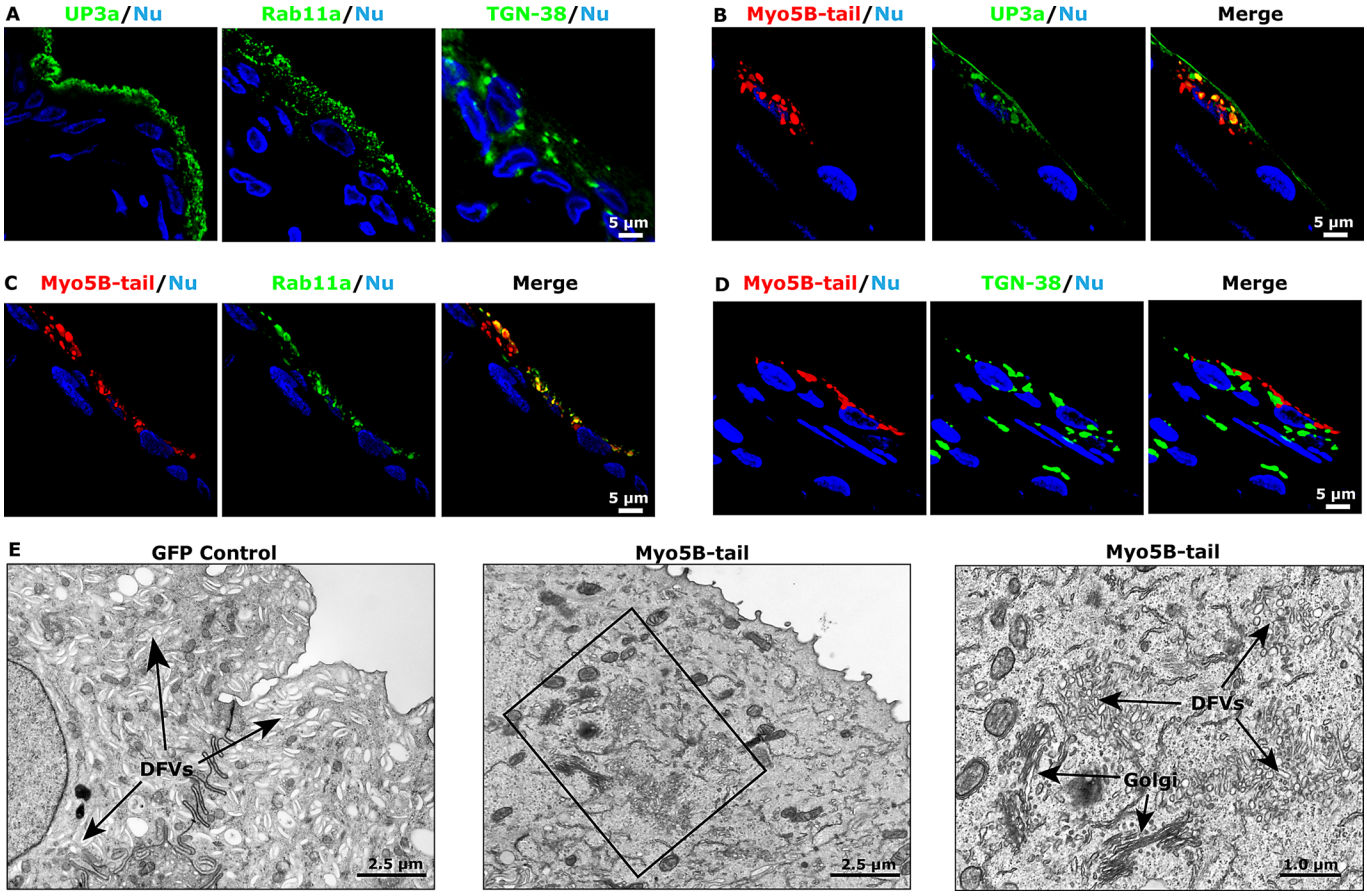

FIGURE 2: Expression of Myo5B-tail clusters DFVs. (A) Localization of endogenous UP3a, Rab11a, or TGN-38 in uroepithelial tissues. (B–D) Rat bladders were transduced with an adenovirus encoding GFP-tagged Myo5B-tail, the bladder tissues were excised and stained, and the localization of the MyoVb-tail and endogenous UP3a (B), Rab11a (C), or TGN-38 (D) was assessed. (E) Ultrastructure of umbrella cells transduced with GFP (left) or GFP-tagged Myo5B-tail (middle and right). The boxed region in the middle is magnified in the image to the right. The positions of DFVs and Golgi stacks are indicated.

observed when dominant-active, GFP-tagged Rab11a-S_{20}V (DA-Rab11a) was expressed (Figure 5A; Khandelwal *et al.*, 2008). Whereas this increase was measured in excised tissue, voiding in vivo is accompanied by a rapid and complete recovery of all added membrane (Khandelwal *et al.*, 2010). Thus any DA-Rab8a (or Rab11a)- induced increase in umbrella cell surface area would likely be counteracted at each cycle of voiding.

Next we determined whether Rab11a and Rab8a acted in the same network to regulate stretch-induced exocytosis. If true, we reasoned that DN-Rab11a should impair DA-Rab8a–stimulated exocytic events and that DN-Rab8a should inhibit DA-Rab11a–dependent increases. Indeed, this is what we observed (Figure 5A). We were unable to evaluate the effects of expressing both DN-Rab8a and DN-Rab11a on exocytosis, as this caused severe defects in transepithelial resistance. Because these experiments do not resolve which GTPase acts upstream of the other, we performed the following analysis. First, we observed that expression of GFP-tagged DN-Rab11a resulted in a reduction in the subapical accumulation and apparent intensity of Rab8-positive vesicles (Figure 5B). In contrast, expression of DN-Rab8a did not appear to impair the apical localization or apparent intensity of Rab11a-positive DFVs (Figure 5C). These results are consistent with the possibility that Rab11a functions upstream of Rab8, possibly by recruiting

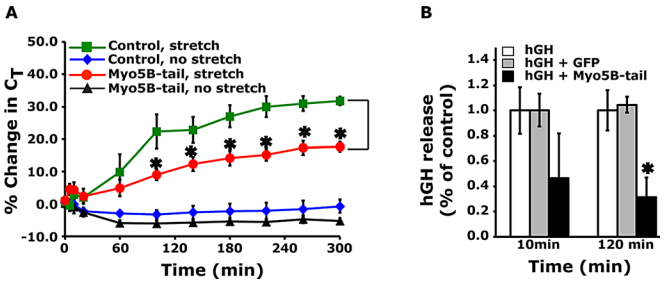

FIGURE 3: Expression of Myo5B-tail impairs stretch-induced exocytosis. (A) Umbrella cells were transduced in situ with adenoviruses expressing GFP (control) or GFP-tagged Myo5B-tail. The excised bladders were mounted in Ussing stretch chambers and either left in a quiescent state (no stretch) or subjected to stretch at $t = 0$. Changes in capacitance (C_T), normalized to the starting value, were recorded. Data are mean ± SEM ($n \geq 6$). Values significantly different from control are indicated with an asterisk. (B) Umbrella cells were transduced with adenoviruses encoding human growth hormone (hGH) alone, hGH and GFP, or hGH and Myo5B-tail. The bladders were then filled, and the release of hGH into the bladder lumen was quantified as described in *Materials and Methods*. Data are mean ± SEM ($n \geq 6$). Values significantly different from control are indicated with an asterisk.

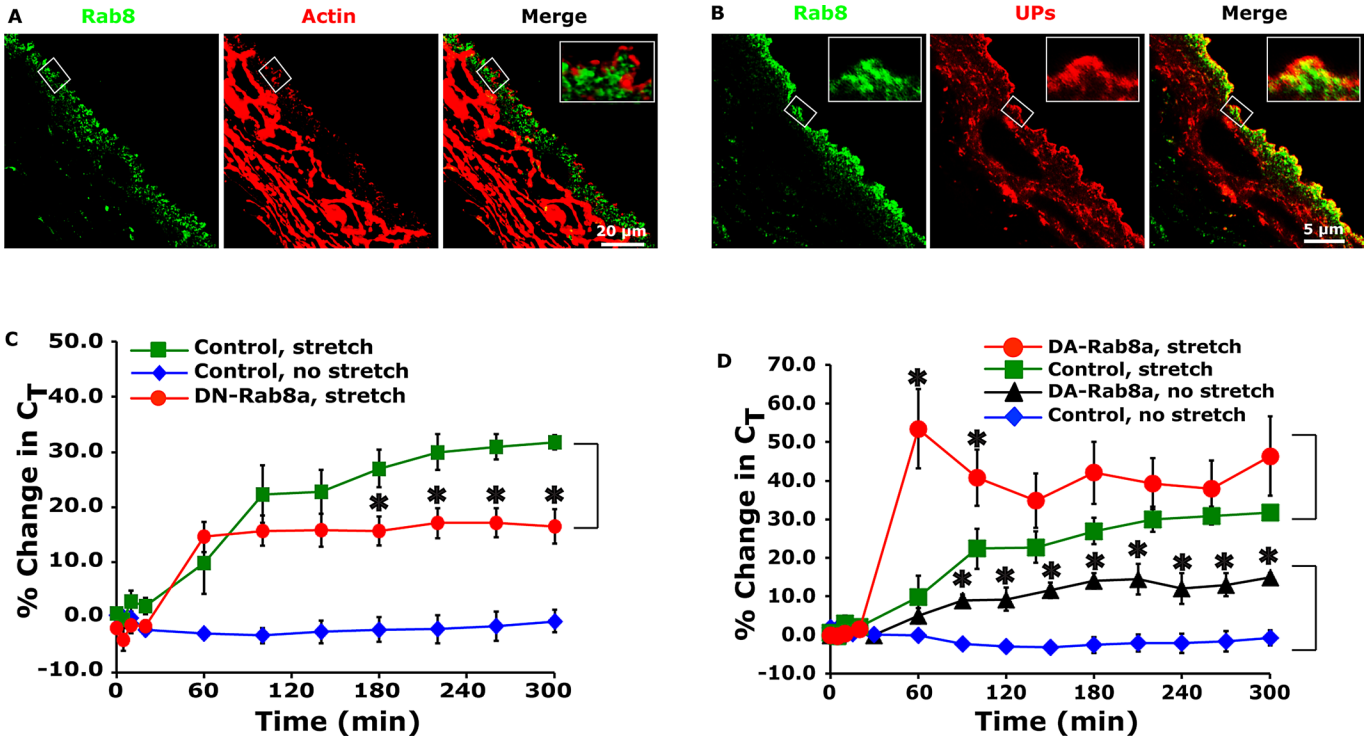

FIGURE 4: Rab8 is associated with DFVs and modulates their exocytosis. (A) Endogenous Rab8 expression in the uroepithelium. Actin was labeled with phalloidin, and nuclei were labeled with ToPro-3. (B) Colocalization of Rab8 and UPs. The latter were labeled with an antiserum that recognize multiple UP species. (C, D) C_T was measured in umbrella cells transduced with GFP (control), GFP-labeled DN-Rab8a, or RFP-labeled DA-Rab8a in the absence or presence of stretch. Data are mean ± SEM ($n \geq 4$). Values significantly different from control are indicated with an asterisk. Control data are reproduced from Figure 3A.

Rab8 to DFVs or by modulating Rab8-positive DFV accumulation at the apical pole of the umbrella cell. Expression of GFP alone did not affect the localization of either Rab8 or Rab11a (Figure 5, B and C).

To further examine the relationship between the Rab8- and Rab11a-positive vesicles and the apical membrane, we performed additional localization studies. In addition to finding Rab8-positive DFVs that were also Rab11a positive (Figure 5D and Table 1), we also observed a pool of Rab8-positive vesicles that appeared to be closer to the apical pole of the cell and thus nearer to the apical plasma membrane. This was more apparent when we compared the distribution of Rab11a and Rab8 to the cytokeratin meshwork. Whereas Rab11a-positive DFVs were mostly found within the network (Figure 5E), those subapical DFVs that were only Rab8 positive were observed outside the cytokeratin meshwork and thus in closer proximity to the apical plasma membrane than Rab11a-positive DFVs (Figure 5F). Unfortunately, we could not find an antibody combination that allowed us to examine the position of Rab8/Rab11a-positive vesicles relative to the cytokeratin meshwork. The proximity of Rab8-positive DFVs to the apical membrane is further evidence that Rab8 may function downstream of Rab11a.

Ciliogenesis and apical lumen formation are both dependent on the Rab11a-dependent recruitment of Rabin8, a GEF that promotes activation and recruitment of Rab8a to Rab11a-positive vesicles (Hattula *et al.*, 2002; Bryant *et al.*, 2010; Knodler *et al.*, 2010). In umbrella cells, Rabin8 appeared in a subapical, punctate distribution (Figure 6A) and colocalized with Rab11a- or Rab8-positive DFVs (Figure 6, B and C, and Table 1). Furthermore, we observed that expression of DN-Rab11a caused endogenous Rabin8 to appear scattered throughout the cytoplasm (Figure 6D), consistent with the possibility that Rabin8 was recruited to DFVs by Rab11a. This effect was not observed in cells expressing DN-Rab8a (Figure 6E). Expression of GFP alone did not alter the distribution of Rabin8 (Figure 6F). Next we examined the effects of expressing wild-type GFP-tagged Rabin8, which we predicted would activate Rab8a and like DA-Rab8a would stimulate exocytosis. Expression of GFP-tagged wild-type Rabin8 had no significant effect in the absence of stretch but significantly increased exocytosis in stretched tissues (Figure 6G). We also expressed a mutant GFP-tagged Rabin8 (Rabin8-L_{196}A/F_{201}A; Rabin8-AA), which lacks Rab8 GEF activity and is believed to act in a dominant-negative manner to suppress Rab8 activation (Park *et al.*, 1997; Bossu *et al.*, 2000). Expression of Rabin8-AA had no effect on the distribution of Rab8, or for that matter of Rab11a or Myo5b (Figure 6, H–J), but like wild-type Rabin8 caused a significant stimulation of stretch-induced exocytosis (Figure 6K). This stimulation was reversed at later time points if Rabin8-AA was coexpressed with DN-Rab8a (Figure 6K), indicating that the Rabin8-AA-mediated increase in exocytosis was at least partially the result of Rab8a-dependent exocytosis. We were unable to assess the effect of coexpressing DN-Rab11a and Rabin8-AA, as this combination caused a large decrease in transepithelial resistance. Taken together, these results indicate that Rabin8 is recruited to DFVs by Rab11a, where it apparently modulates stretch-induced exocytosis in a manner that is independent of its GEF activity.

Relationship between Myo5B and Rab8a- and Rab11a-dependent DFV exocytosis

To determine the relationship of Myo5B to the Rab11a-Rab8 network, we first examined the effects of coexpressing the Myo5B-tail

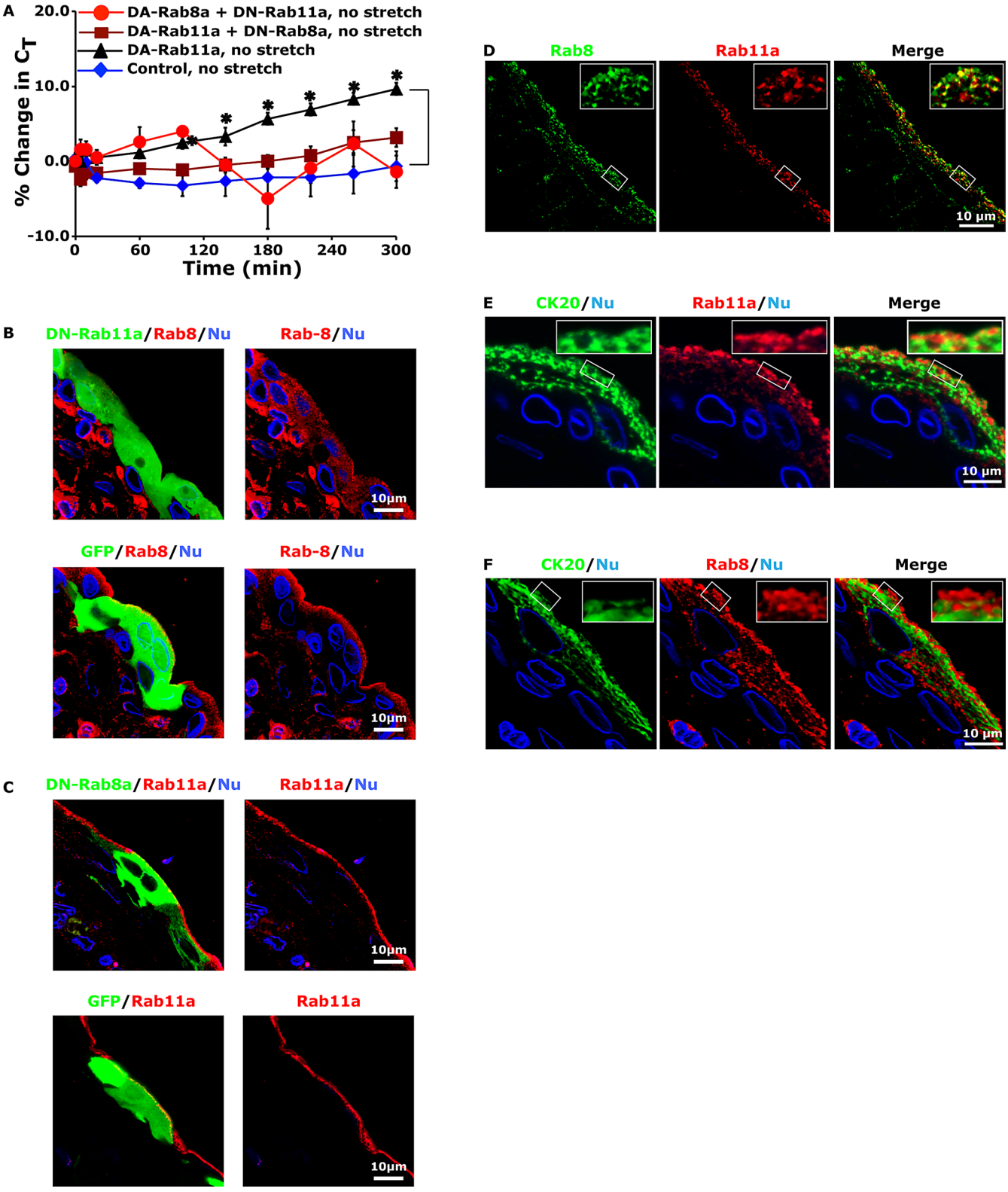

FIGURE 5: Rab8a acts downstream of Rab11a to modulate DFV exocytosis. (A) Umbrella cells were transduced with GFP (control) or with the indicated constructs. The percentage change in C_T was monitored in unstretched, quiescent bladders and recorded. Data are mean ± SEM ($n \geq 4$). Values significantly different from control are indicated with an asterisk. The control, no-stretch data in Figure 3A are reproduced in A. (B) Effect of expressing GFP-tagged DN-Rab11a (top) or GFP alone (bottom) on Rab8 localization in umbrella cells. (C) Umbrella cells were transduced with GFP-tagged DN-Rab8a (top) or GFP alone (bottom), and the localization of Rab11a was examined in cross sections of bladder tissue. (D) Colocalization of endogenous Rab8 and Rab11a in the uroepithelium. (E, F) Distribution of Rab11a (E) or Rab8 (F) and the apical cytokeratin network labeled with an antibody to CK20. Nuclei were labeled with an anti–lamin B receptor antibody.

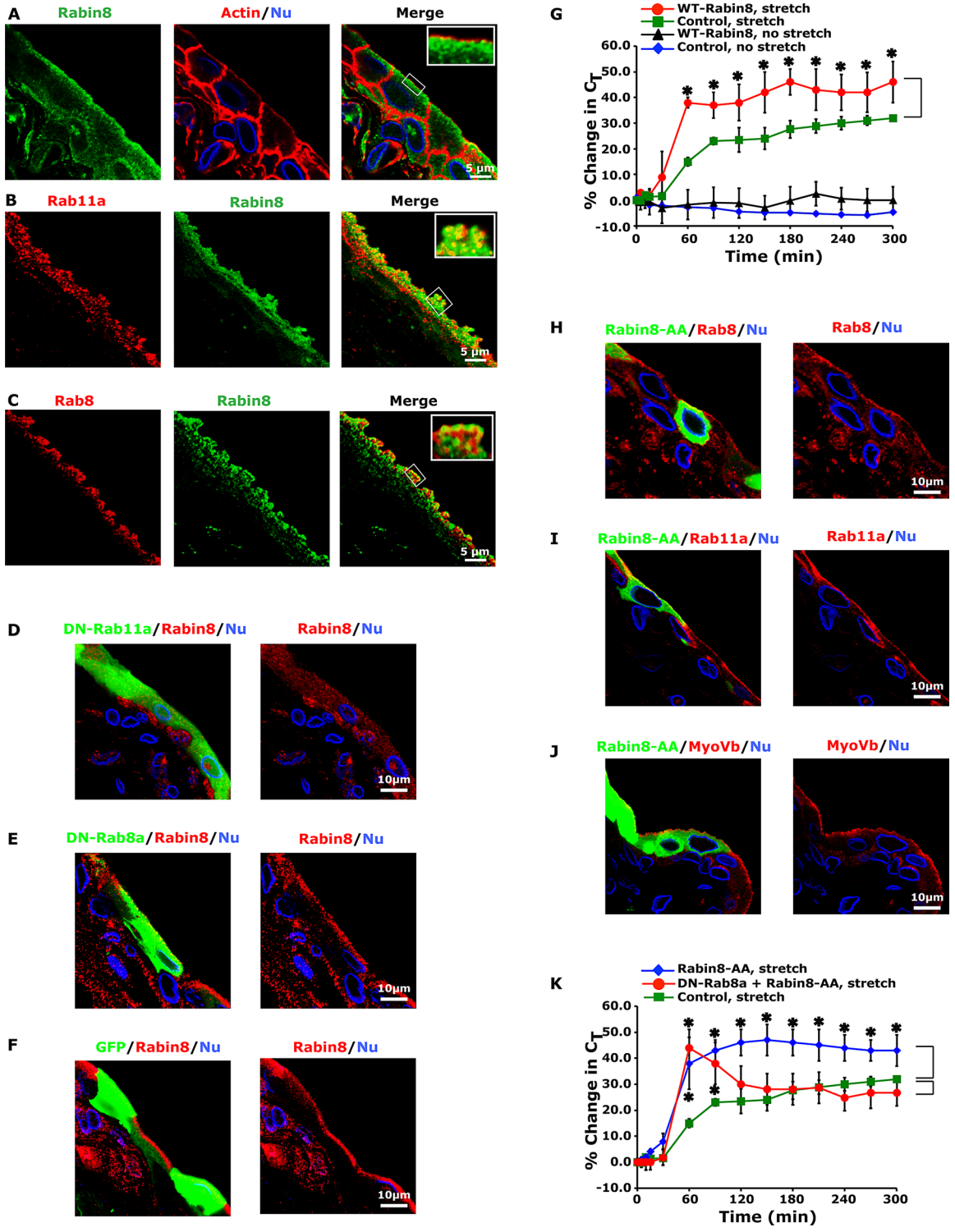

FIGURE 6: Localization of Rabin8 and effects of expressing wild-type (WT), GFP-tagged Rabin8, or Rabin8-AA on exocytosis. (A) Localization of endogenous Rabin8, actin, and nuclei in the rat uroepithelium. (B, C) Colocalization of endogenous Rabin8 with Rab11a (B) or Rab8 (C). The tissue in B and C is more stretched than that in A. (D–F) Bladders were transduced in situ with adenoviruses encoding GFP-tagged DN-Rab11 (D), GFP-tagged DN-Rab8a (E), or GFP alone (F) and the endogenous distribution of Rabin8 assessed. (G) Bladders transduced in situ with GFP alone (control) or GFP-tagged Rabin8 were mounted in Ussing chambers and then left in a quiescent state (no stretch) or stretched. The percentage change in C_T is reported. Data are mean ± SEM ($n \geq 4$). Values significantly different from control are indicated with an asterisk. Control data are reproduced from Figure 3A. (H–J) Localization of endogenous Rab8 (H), Rab11a (I), or Myo5B (J) in issue transduced with GFP-tagged Rabin8-AA. (K) Umbrella cells were transduced with viruses encoding GFP, GFP-tagged Rabin8-AA, or both GFP-tagged Rabin8-AA and DN-Rab8a. The bladders were stretched at $t = 0$. The percentage change in C_T is reported. Data are mean ± SEM ($n \geq 4$). Values significantly different from control are indicated with an asterisk. The control, stretch data are reproduced from Figure 3A.

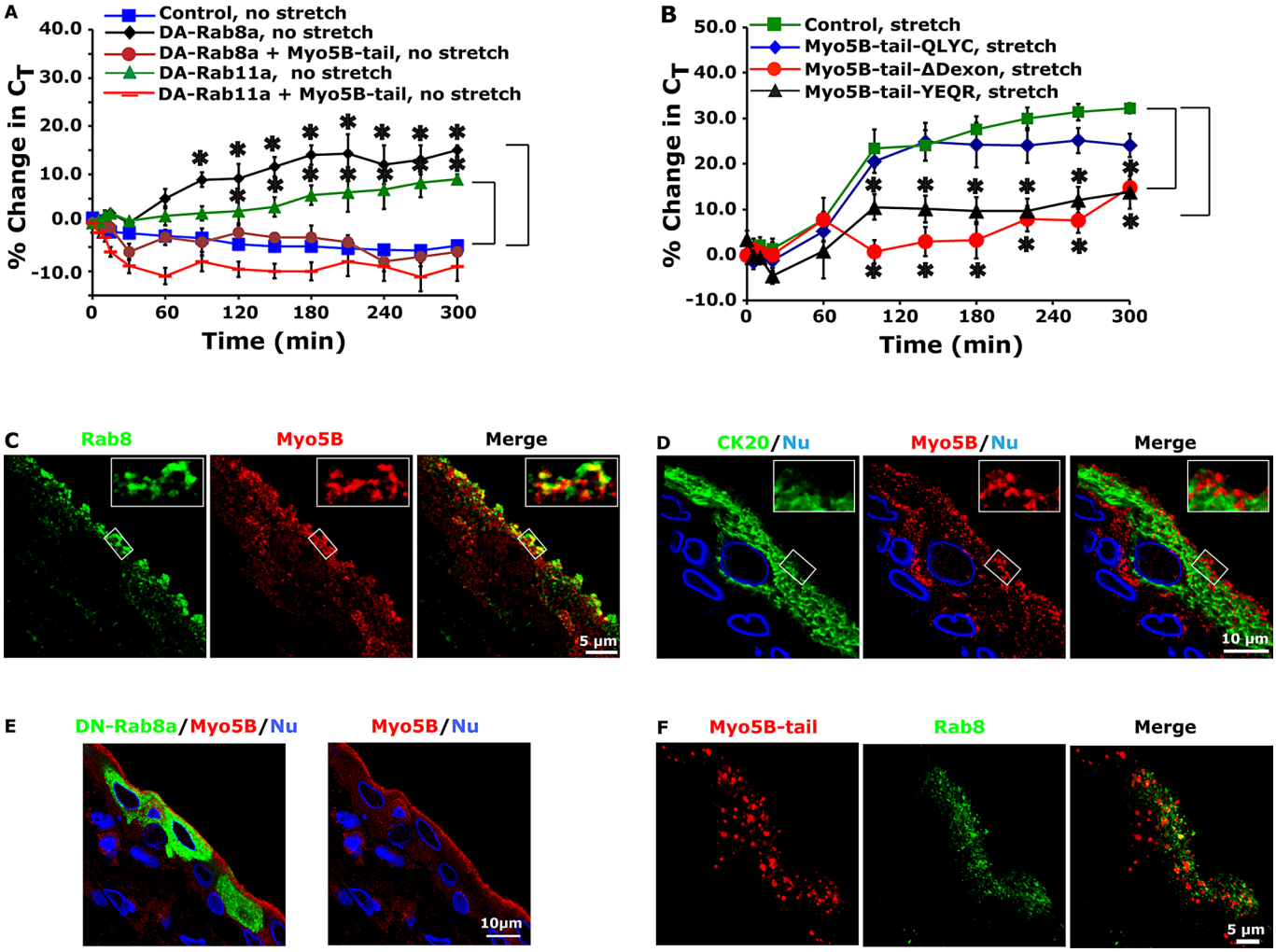

FIGURE 7: Rab11a and Rab8a act together with Myo5B to regulate DFV exocytosis. (A) Umbrella cells were transduced with GFP alone (control) or GFP-tagged DA-Rab8a or DA-Rab11a in the presence or absence of GFP-tagged Myo5B-tail. The percentage change in C_T was monitored in isolated quiescent bladders. Data are mean ± SEM ($n \geq 4$). Values significantly different from control are indicated with an asterisk. DA-Rab8a, no stretch, DA-Rab11a, no stretch, and control, no stretch are reproduced from Figures 4D, 5A, and 3A, respectively. (B) Umbrella cells were transduced with GFP (control) or the indicated GFP-tagged Myo5B-tail mutant. The percentage change in C_T was recorded for bladder tissue mounted in Ussing stretch chambers and subjected to stretch. To aid comparisons, the control, stretch data from Figure 3A are reproduced. Data are mean ± SEM ($n \geq 5$). Values significantly different from control are indicated with an asterisk. (C, D) Colocalization of endogenous Myo5B with Rab8 (C) or CK20 (D). (E) Effect of expressing GFP-tagged DN-Rab8a on the distribution of Myo5B. (F) Umbrella cells were transduced with virus encoding GFP-tagged Myo5B-tail. The distributions of Rab8 and GFP-tagged Myo5B-tail are shown.

with either DA-Rab8a or DA-Rab11a. We observed that Myo5B-tail impaired the ability of these mutants to stimulate increases in DFV exocytosis (Figure 7A), indicating that Myo5B acted within the same network as Rab11a and Rab8a. Next we sought to determine which GTPase acted upstream of Myo5B to promote DFV exocytosis. We expressed mutant Myo5B cargo-binding domains that cannot form interactions with either Rab8a, or Rab10, or Rab11a (Figure 7B; Roland *et al.*, 2011). Myo5B does not interact with Rab8b (Roland *et al.*, 2007). In the simplest case, for example, when Myo5B acts solely downstream of Rab11a, we expected that wild-type Myo5B-tail (or mutants lacking the Rab8a or Rab10 interaction sites) would inhibit exocytosis, whereas a mutant lacking the Rab11a interaction site (Myo5B-tail-YEQR) would not. Surprisingly, Myo5B-tail-YEQR inhibited these trafficking events (Figure 7B). Likewise, Myo5B-tail-ΔD_{exon}, which lacks the D exon of the protein and does not interact with Rab10, also impaired exocytosis (Figure 7B). In contrast, the Myo5B-tail-QLYC, which cannot interact with Rab8a, failed to block stretch-induced exocytosis (Figure 7B), indicating that Myo5B may be acting downstream of this GTPase. Consistent with the latter possibility, we measured some overlap between Myo5B and Rab8 (Figure 7C and Table 1) and also noted that, like Rab8, a population of Myo5B-positive vesicles extended beyond the cytokeratin matrix and were in close apposition to the plasma membrane (Figure 7D).

However, other studies indicated that the interplay between Myo5B and Rab8a was more complex than a simple one-on-one interaction. First, as noted previously, there was a population of Rab11a-positive DFVs that were also positive for Myo5B (Figure 1E). Furthermore, expression of the Myo5B-tail caused Rab11a-positive vesicles to cluster (Figure 2C). Second, the subapical distribution of Myo5B was not obviously affected by expression of DN-Rab8a

(Figure 7E). Furthermore, Rab8-positive vesicles showed only a small degree of colocalization with Myo5B-tail–induced clusters (Figure 7F; Manders' coefficient $M_Y = 0.23 \pm 0.07$), and almost no colocalization was measured when the intensities of the Myo5B-tail clusters were compared with those for Rab8 ($M_X = 0.04 \pm 0.01$; Table 1). However, we did note that Rab8-positive DFVs appeared dispersed and fragmented under these conditions. Similar results were obtained for Rabin8 (Table 1). In sum, the data indicate a role for Myo5B within the Rab8a/Rab11a network; however, the interaction is likely to be more complex than a simple recruitment of Myo5B by one or the other GTPase in this module.

DISCUSSION

Our studies show that Rab11a, which we previously implicated in DFV exocytosis (Khandelwal *et al.*, 2008), acts as a partner in a connected network of proteins that also likely includes Rab8a and Myo5B. A Rab11-Rab8-Myo5B network has been described for the biogenesis of cilia and apical lumen formation (Bryant *et al.*, 2010; Knodler *et al.*, 2010), and a homologous Ypt31/32p-Sec4p-Myo2p yeast pathway has been implicated in yeast exocytosis (Ortiz *et al.*, 2002; Medkova *et al.*, 2006; Jin *et al.*, 2011). However, the connection of these conserved pathways to regulated secretion was not previously appreciated.

In ciliogenesis, in lumen formation, and in the yeast secretory system, the Rab11–Rab8 network is believed to be arranged as a "cascade" that promotes a process termed Rab conversion or maturation (Rink *et al.*, 2005; Hutagalung and Novick, 2011). During this conversion, Rab11 present on an upstream compartment engages a GEF for Rab8 (e.g., Rabin8), stimulating Rab8's conversion from an inactive, GDP-bound state to an active, GTP-bound state and recruitment to the membrane (Knodler *et al.*, 2010). In its GTP-bound state, active Rab8 recruits effector proteins to the compartment, modifying its membrane and further promoting vesicular movements and fusion (Barr and Lambright, 2010). Effectors include specific GTPase-activating proteins (GAPs), which, when recruited by Rab8, promote the transformation of GTP-bound Rab11 to its GDP-bound state, preserving compartmental identity by inactivation of the upstream Rab (Rivera-Molina and Novick, 2009; Barr and Lambright, 2010; Bryant *et al.*, 2010). Rab cascades have been described for pathways that involve endosomes (Eitzen *et al.*, 2000; Rink *et al.*, 2005; Zhu *et al.*, 2009; Bryant *et al.*, 2010; Poteryaev *et al.*, 2010), in addition to those described for the constitutive secretory pathway (Ortiz *et al.*, 2002; Morozova *et al.*, 2006; Rivera-Molina and Novick, 2009; Starr *et al.*, 2010; Grigoriev *et al.*, 2011).

Although we have not identified the relevant GAPs and GEFS in DFV exocytosis, the ability of DN-Rab11a to effect the distribution of Rab8a, but not vice versa, the differential proximity of Rab11a versus Rab8 vesicles to the apical plasma membrane, and the homology to similarly organized pathways are consistent with the possibility that DFV exocytosis may also be regulated by a Rab cascade. Additional support for this possibility is the finding that DFVs undergo a maturation process as they exit from the TGN and their lumens become increasingly acidic (Guo *et al.*, 2009), and in rodents (but not humans or rabbits), a shape change occurs as DFVs transition from discoidal shaped to one that is fusiform in appearance as they move toward the apical pole of the cell (Hudoklin *et al.*, 2009, 2012). Superimposed on this maturation is DFV transport to the surface, which depends, in part, on a dense subapical cytokeratin network, which encases the DFVs and in response to filling moves the enmeshed vesicles toward the apical pole of the cell as the cytokeratins are "pulled" from a random orientation to one that aligns parallel to the apical surface of the umbrella cell (Truschel *et al.*, 2002; Veranic and Jezernik, 2002). DFVs must then move through the subapical actin cytoskeleton, which we describe in this study, before soluble *N*-ethylmaleimide–sensitive factor attachment protein receptor (SNARE)–dependent fusion with the apical membrane (Born *et al.*, 2003).

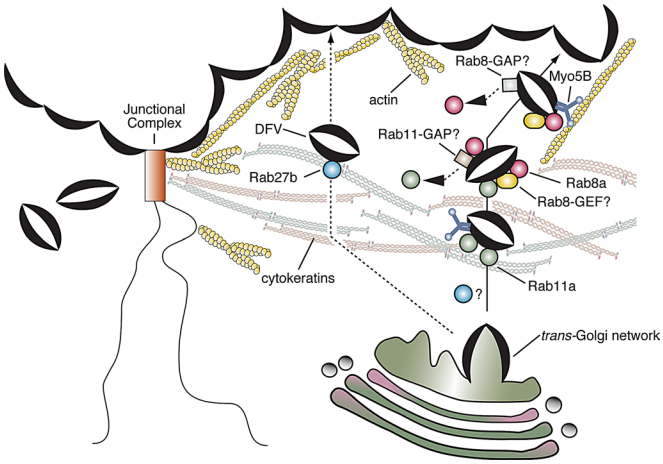

FIGURE 8: Model for hypothesized role of the Rab11a-Rab8a-Myo5B network in regulating DFV exocytosis. Newly synthesized DFVs exit the TGN, where they associate with Rab11a, which may facilitate DFV passage through the cytokeratin meshwork. In one scenario, Rab11a may promote early recruitment of the Myo5B motor. In addition, Rab11a stimulates DFV maturation by recruiting Rab8a to the vesicles. The GEF is unknown but is apparently not Rabin8, which is recruited to DFVs by Rab11a and may modulate exocytosis through other effector proteins (not shown). In turn, Rab8a recruits an unknown Rab11a GAP, which would terminate the Rab11a-dependent steps and maintain compartment identity. Myo5B may also be recruited by Rab8a, but the interaction is likely to be ephemeral and may be stabilized by other proteins, including the exocyst subunit Sec15 and SNARE proteins (not shown). An important function of Myo5B is to promote DFV transit through the subapical actin cytoskeleton before fusion.

Because Rab11a does not colocalize with the umbrella cell TGN (Khandelwal *et al.*, 2008) and Rab11a-positive DFVs are generally encased within the subapical cytokeratin cytoskeleton, we hypothesize that Rab11a acts subsequent to DFV release from the TGN and may be important in modulating vesicle transit through the cytokeratin meshwork and the initial aspects of the subapical actin network (Figure 8). In addition, Rab11a likely fosters DFV maturation by recruiting the downstream Rab8a GTPase. The mechanism by which Rab11a recruits Rab8a in umbrella cells is unknown. Whereas Rabin8 is apparently recruited to DFVs downstream of Rab11a, it is unlikely to be the relevant Rab8 GEF because its overexpression stimulates exocytosis irrespective of its GEF activity. How it does so is unclear, but it is possible that the amount of Rabin8 is normally limiting and overexpression potentiates interactions with binding partners, which positively regulate the Rab11a–Rab8a pathway in umbrella cells (independent of Rabin8's GEF activity). Alternatively, the Rabin8-interacting proteins may act as negative regulators of exocytosis, and binding to Rabin8 relieves this inhibition. Although the target of Rabin8 in DFV exocytosis is unknown, studies reported interactions between Rabin8 and Rab3a, Rheb, SSX2, ad Sec15 (Brondyk *et al.*, 1995; de Bruijn *et al.*, 2002; Parkhitko *et al.*, 2011; Feng *et al.*, 2012). Finally, if we assume a Rab cascade is operative, then after its recruitment, Rab8a is likely to enlist a Rab11a GAP, the identity of which is unknown but may include putative Rab11a GAPs described in other studies (Fukuda, 2011). Although a Rab cascade

is attractive, we cannot rule out the possibility that the Rab11a–Rab8a network we describe here may be organized in a manner more complex than a cascade of sequential events.

The other player in DFV exocytosis we identified is Myo5B, which our studies indicate may work in conjunction with Rab8a and possibly Rab11a to ensure DFV passage through the subapical cortical actin cytoskeleton (Figure 8). However, it is possible that Myo5B may function at other actin-dependent steps that precede delivery to the apical membrane (see later discussion). Myo5B is a well-known effector of Rab11a (Lapierre *et al.*, 2001; Volpicelli *et al.*, 2002; Wakabayashi *et al.*, 2005; Varthakavi *et al.*, 2006; Nedvetsky *et al.*, 2007; Swiatecka-Urban *et al.*, 2007; Provance *et al.*, 2008; Chu *et al.*, 2009; Roland *et al.*, 2011; Schuh, 2011; Xu *et al.*, 2011), but more recent data indicate that it can also interact with Rab8a (but not Rab8b) and Rab10 (Roland *et al.*, 2007, 2011). Indeed, we observed colocalization between Rab11a and Myo5B, as well as colocalization between Myo5B and Rab8. Furthermore, Myo5B was associated with vesicles that were in close proximity to the plasma membrane. We also noted that a Myo5B-tail mutant lacking an Rab11a-interacting motif (Myo5B-tail-YEQR) impaired exocytosis. In contrast, a mutant Myo5B-tail that lacked an Rab8a-interacting motif (Myo5B-tail-QLYC) failed to inhibit exocytosis. In the simplest scenario, in which MyoVb forms an interaction with only the Rab8 GTPase, these results would indicate that a Rab8a–Myo5B interaction was critical for this process. However, interactions between Myo5 family motors and both Rab8 and Rab11 homologues have been reported in both yeast and mammalian cells (Lipatova *et al.*, 2008; Jin *et al.*, 2011). Thus an additional scenario, which may better fit our data, is that Myo5B forms interactions with both GTPases (Figure 8). This would explain why a fraction of Rab11a colocalizes with Myo5B and why Myo5B-tail clusters Rab11a-positive DFVs. In this second scenario, Myo5B-tail-YEQR would inhibit DFV exocytosis by perturbing the interaction between Myo5B and the downstream Rab8a GTPase. In contrast, expression of Myo5B-tail-QLYC, which retains its Rab11a-interacting motif, would primarily affect the upstream, Rab11a-dependent reaction, and not the downstream Rab8a one. On the assumption that sufficient Rab8a-positive DFVs were available under these conditions, their exocytosis would proceed, apparently unimpeded by expression of this mutant.

We also observed that Rab8-positive vesicles were not efficiently recruited into Myo5B-induced clusters and that expression of DN-Rab8a failed to affect the distribution of Myo5B. At first take, these observations appear to be inconsistent with a role for Rab8a in recruiting Myo5B. However, some provisos are worth noting. First, expression of Myo5B-tail was not without effect, as the Rab8-positive vesicles appeared smaller and dispersed in their distribution. Second, in cells expressing Myo5B-tail the affinity of Rab8a for Myo5B may be less than that of Rab8a for other interacting proteins such as Myo5A (Roland *et al.*, 2007), which is also expressed in umbrella cells. If so, Myo5A (or other interacting partners) may "pull" Rab8 out of the Myo5B-induced clusters or prevent Rab8a-positive vesicles from being incorporated into these clusters. Additional Rab8a-interacting proteins include Rab11a. Furthermore, the yeast Myo2p motor interacts with the Sec15 subunit of the exocyst, an octomeric complex that may promote vesicle tethering before fusion with the plasma membrane (Jin *et al.*, 2011), and other Myo5 motors interact with SNARE components, including syntaxins and vesicle-associated membrane proteins (Prekeris and Terrian, 1997; Watanabe *et al.*, 2005; Bond *et al.*, 2011). Any one or combination of these proteins could act to effect Myo5B localization in the absence of Rab8a. Although our studies support an important role for Myo5B in DFV, additional studies are needed to understand the relationship of Myo5B to Rab11a/Rab8a-dependent DFV exocytosis. Finally, Myo5A can also form interactions with Rab8, Rab11, and Rab27 (Roland *et al.*, 2007; Rudolf *et al.*, 2011), so this motor may also play an important role in DFV exocytosis.

In addition to Rab11a and Rab8a, Rab27b is also reported to interact with a subset of DFVs (Chen *et al.*, 2003). Technically, Rab27b could act upstream or downstream of this Rab11a/8a network; however, we previously reported that there are at least two populations of DFVs: a preexisting pool that undergoes rapid exocytosis, and one that requires new protein synthesis and only slowly fuses with the apical membrane (Balestreire and Apodaca, 2007; Yu *et al.*, 2009). Therefore it is possible that Rab27b associates with one of these vesicle pools and Rab11a/8a with the other. This could also explain why none of the dominant-negative constructs we used gave an all-or-none response and may also speak to possible Rab targets of Rabin8 that may modulate the Rab11a/8a pathway.

An important prediction of our work is that Rab/myosin motor networks and possibly cascades will be common to other regulated secretory system. Support for this proposition includes the following: 1) Purified synaptic vesicles, insulin secretory granules, and zymogen granules contain 10–30 Rabs (Takamori *et al.*, 2006; Brunner *et al.*, 2007; Rindler *et al.*, 2007). Putting aside the possibility that contamination with other organelles contributes to this tally, multiple, sequentially acting Rabs would ensure that the complex process of secretory granule maturation occurs in an orderly and vectorial manner and that exocytosis is properly timed and of the correct duration. 2) Exocytosis in neuroendocrine cells requires Rab3 isoforms (Fukuda, 2008; Pavlos and Jahn, 2011). However, neurons lacking expression of all four Rab3 isoforms only show a 30% loss of stimulated neurotransmitter release (Schluter *et al.*, 2004). Thus other Rabs, most likely Rab27 isoforms, are likely to be involved (Fukuda, 2008; Pavlos and Jahn, 2011). Of interest, Rab3 and Rab27 share effectors and GEFs, and both act at late stages in the regulated exocytic response (Tsuboi and Fukuda, 2006; Handley *et al.*, 2007; Pavlos *et al.*, 2010; Pavlos and Jahn, 2011). 3) Myosin motors, particularly Myo5A, are common requirements for regulated secretion (Rudolf *et al.*, 2011), and, as noted, can promote vesicle motility as well as vesicle tethering and fusion. Based on our insights into umbrella cell exocytosis, it is likely that Rab3 and Rab27 also form a Rab cascade or network, and their sequential functions will be important in modulating the broad array of regulated secretory pathways that depend on these proteins for their function (Fukuda, 2008).

MATERIALS AND METHODS

Reagents and antibodies

Unless specified otherwise, all chemicals were obtained from Sigma-Aldrich (St. Louis, MO). Polyclonal antibodies and mouse monoclonal 8H10 antibody to Rab11a have been described (Lapierre *et al.*, 2003). Other antibodies included rabbit anti–human growth hormone (hGH; National Hormone and Peptide Program, Torrance, CA) or mouse monoclonal anti-hGH (BD Biosciences, San Jose, CA), mouse monoclonal K8B12 antibody against UP3a (Truschel *et al.*, 2002), rabbit anti–TGN-38 (Sigma-Aldrich), rabbit anti-Myo5B (a kind gift from Irwin Arias and John Hammer, National Institutes of Health, Bethesda, MD), mouse monoclonal anti-Rab8 (BD Biosciences), mouse anti–cytokeratin 20 (Dako, Carpinteria, CA), goat anti–lamin B receptor (Acris, San Diego, CA), or rabbit anti–asymmetric unit membrane antibody (kindly provided by T. T. Sun, New York University, New York, NY). A rabbit polyclonal Rabin8/Rab3a-interacting protein antibody was produced as described previously (Hattula *et al.*, 2002) or purchased from LifeSpan Biosciences (Seattle, WA; LS-C120290).

Fluorophore- or horseradish peroxidase–labeled, affinity-purified and minimal cross-reacting goat or donkey secondary antibodies were purchased from Jackson ImmunoResearch (West Grove, PA). Rhodamine phalloidin and TO-PRO3 were obtained from Molecular Probes-Invitrogen (Grand Island, NY).

Animals

Urinary bladders were obtained from female Sprague Dawley rats (250–300 g). Rats were killed by inhalation of 100% CO_2, followed by a thoracotomy. All animal studies were approved by the University of Pittsburgh Institutional Animal Care and Use Committee.

RT-PCR

The uroepithelium was recovered by gentle scraping as described (Balestreire and Apodaca, 2007), the cells were lysed, and RNA was purified using the RNAqueous Micro Kit (Life Technologies, Carlsbad, CA). RNA was treated with DNase I and cDNA generated using the RETROscript First Strand Synthesis Kit (Life Technologies). PCR was performed using Taq polymerase (Life Technologies). The primers used were as follows: Myo5A, GTG GGG CAA AAG AGA C and TCA GAC CCT TGC AAT GAA GCC; Myo5B, GCA GCC CAA CTC CTT CAG and TCA GAC TTC ATT GAG GAA CTC; Rab8a, ATG GCG AAG ACC TAC GAT TAC C and TCA CAG GAG ACT GCA CCG G; and Rab8b, ATG GCG AAG ACG TAC GAT TAT CTG and TCA AAG CAG AGA ACA CCG GAA G. Sequencing was used to confirm the identity of the PCR reaction products.

Preparation of adenoviruses and in situ transduction of umbrella cells

Adenoviruses expressing GFP, GFP-tagged DN-Rab11aS_{25}N, DA-Rab11aS_{20}V, and hGH were described previously (Khandelwal *et al.*, 2008). GFP-tagged Myo5B-tail mutants showing reduced affinity for Rab8a (Myo5B-QLYC), Rab10 (Myo5B-ΔD_{exon}), or Rab11a (Myo5B-YEQR) were described previously (Roland *et al.*, 2011). Adenoviruses were made by cloning the appropriate cDNAs into the plasmid pAdlox. Rab8a was cloned into pAdlox, and adenoviruses expressing RFP-tagged DA-Rab8aQ_{67}L and GFP-tagged DN-Rab8aT_{22}N were made by mutating Glu_{67} to Lys and Ser_{22} to Val in Rab8a-pAdlox using the QuikChange Site-Directed Mutagenesis Kit (Agilent, Santa Clara, CA). cDNA for human Rabin8a was obtained from Addgene (Cambridge, MA) and subcloned into pAdlox. The QuikChange Kit was then used to generate the Rabin8a-F_{201}A/L_{196}A mutant. Adenoviruses were prepared and purified, and bladders were transduced in situ using our previously described methods (Khandelwal *et al.*, 2008).

Estimation of hGH secretion

Rat bladders were transduced in situ with adenoviruses expressing hGH alone or in combination with Myo5B-tail or GFP. The bladders were filled, and hGH released into the bladder lumen was collected and Western blots quantified as described (Khandelwal *et al.*, 2008).

Mounting rat bladder in Ussing stretch chambers and measuring C_T

Rats were killed, and bladders were excised, cut open, and then mounted in a Ussing stretch chamber with the mucosal surface facing an enclosed stretch hemichamber (Khandelwal *et al.*, 2008). After a 1-h period of equilibration, bladder filling was simulated by slowly adding Krebs buffer to the mucosal hemichamber. The chamber was then sealed, and an additional solution was added to further stimulate DFV exocytosis and fusion. Changes in the umbrella cell surface area were monitored by measuring C_T as previously described (Khandelwal *et al.*, 2008).

Immunofluorescence labeling, image acquisition, and measurement of colocalization

Bladder tissue was fixed and processed as described (Khandelwal *et al.*, 2008); however, the Rab8 antibody only reacted if the following procedure was followed. After the frozen tissue was cross-sectioned and rehydrated with phosphate-buffered saline (PBS), we performed antigen retrieval by incubating the tissue for 7 min with quench buffer (20 mM glycine, pH 8.0, and 75 mM NH_4Cl dissolved in PBS) containing 0.1% Triton X-100. This was followed by a 3-min incubation in quench buffer containing 0.05% SDS and 0.1% Triton X-100. The tissue was then quickly rinsed three times with PBS and then three times for 5 min in the same buffer. When mounting the tissues, we found that enhanced image quality could be obtained if postfixation the tissues were rinsed with 100 mM Tris, pH 8.0, and then treated for 1–2 min each with ascending concentrations of thiodiethanol (50, 75, and 97% [vol/vol]) dissolved in the same buffer (Staudt *et al.*, 2007). The samples were then mounted in 97% thiodiethanol/Tris buffer containing 0.01% (wt/vol) phenylenediamine and stored at −20°C. The 97% thiodiethanol has the same refractive index as our immersion oil (1.1518). Although this solution worked well for proteins labeled with secondary antibodies, tetramethylrhodamine isothiocyanate–phalloidin and To-Pro3 were quickly leached out the samples, necessitating the use of our standard glycerol-based mounting medium for these markers (Acharya *et al.*, 2004). Images were captured using an HCX PL APO 63×/numerical aperture (NA) 1.3 glycerol objective (Leica, Wetzlar, Germany) or a Leica STED 100×/NA 1.4 oil objective and the appropriate laser lines of a Leica TCS SP5 CW-STED confocal microscope (in normal confocal mode). The photomultipliers were set at 900–1200, and 8-bit images were collected using four to eight line averages combined with four to eight frame averages. Serial 0.25-µm *z*-sections were acquired. The images were imported into Volocity 4D software (PerkinElmer, Waltham, MA) and, after image reconstruction, exported as TIFF files. The contrast of the latter was corrected in Photoshop CS5 (Adobe, San Jose, CA), and the composite images were prepared in Adobe Illustrator CS5.

Measures of colocalization were performed using Volocity software, and Manders' colocalization coefficients were calculated as previously described (Khandelwal *et al.*, 2008). Briefly, stacks of dual-labeled confocal sections were imported into Volocity, background noise was removed using the fine (3 × 3) median noise reduction filter, and a scatter plot of green and red pixel intensities (associated with each of the two markers in question) was generated using the colocalization function. A constant threshold of 40 was applied to both channels of the image stack, and Manders' colocalization coefficients for each of two markers (M_X and M_Y, respectively) were calculated for the entire three-dimensional image stack using the following equations (Manders *et al.*, 1993):

$$M_X = \frac{\sum_i X_{i,\text{colocalized}}}{\sum_i X_i} \quad \text{and} \quad M_Y = \frac{\sum_i Y_{i,\text{colocalized}}}{\sum_i Y_i}$$

where X_i is equal to the intensity of marker X at a given voxel and $X_{i,\text{colocalized}} = X_i$ if the associated intensity of the other marker (Y_i) is above the threshold value (i.e., it colocalizes). However, $X_{i,\text{colocalized}} = 0$ if Y_i is below the threshold value (i.e., does not colocalize). Y_i is equal to the intensity of marker Y at a given voxel and $Y_{i,\text{colocalized}} = Y_i$ if X_i is above the threshold value and $Y_{i,\text{colocalized}} = 0$ if X_i is

below the threshold value. An M_X (or M_Y) value of 1.0 indicates that the ratio for all *X* intensity values that have a corresponding *Y* intensity (i.e., are colocalized), divided by the sum of all *X* intensity values is 100%. In contrast, a value of 0.0 indicates that there is no colocalization. We previously reported combinations of markers that had minimal colocalization (Khandelwal *et al*., 2008, 2010), and for this study we colocalized MyoVb and nuclei, which had minimal overlap and resulted in a coefficient that approached zero (see Table 1). The values for M_X and M_Y can be similar or not, as the values are intensity weighted, and in addition one marker may have a broader distribution than the other in the sampled region of the tissue.

Electron microscopy

Bladder tissue was isolated and then fixed with 2.0% (vol/vol) glutaraldehyde and 2% (wt/vol) paraformaldehyde in 100 mM sodium cacodylate buffer, pH 7.4, containing 0.5 mM $MgCl_2$ and 1 mM $CaCl_2$ for 60 min. The tissue was then cut into small pieces, washed with 100 mM sodium cacodylate, pH 7.4, cut into small blocks (2–5 mm in size), and then postfixed in 1.0% (wt/vol) OsO_4 and 1.0% (wt/vol) $K_4Fe(CN)_6$, in 100 mM sodium cacodylate, pH 7.4. After a wash with water, the samples were en bloc stained overnight in 0.5% (wt/vol) uranyl acetate. The tissues were then dehydrated in a graded series of ethanol, and after incubation in propylene oxide, embedded in the epoxy resin LX-112 (Ladd, Burlington, VT) and cured 2 d at 60°C. Embedded tissue was sectioned with a diamond knife (Diatome, Fort Washington, PA), and sections, silver to pale gold in color, were mounted on Butvar-coated nickel grids, contrasted with uranyl acetate and lead citrate, and viewed at 80 kV in a 100 CX electron microscope (JEOL, Tokyo, Japan). Images were captured using an L9C Peltier-cooled transmission electron microscopy camera system (Scientific Instruments and Applications, Duluth, GA). Digital images were imported into Adobe Lightroom, and the images were processed by using the brightness, contrast, and clarity controls. When contrast was too low, adjustments to the tone curve were made to the whole image. Images were sharpened using a radius of 0.5, and luminance noise reduction was performed. The composite images were assembled using Adobe Illustrator CS5.

Statistical analysis

Data are reported as mean ± SEM. Statistically significant differences between means were determined using a two-tailed Student's *t* test; $p < 0.05$ was considered statistically significant. One-way analysis of variance, with Bonferonni's correction, was used when making multiple comparisons.

ACKNOWLEDGMENTS

We thank T. T. Sun, Irwin Arias, and John Hammer for their kind gifts of antibodies. This work was supported by an American Heart Association Scientist Development Grant (to P.K.), National Institutes of Health Grants R37-DK54425, R01-DK077777, and P30-DK079307 (to G.A.) and R01-DK048370 and R01-DK070856 (to J.G.), and the Cellular Physiology and Kidney Imaging Cores of the Pittsburgh Center for Kidney Research (P30-DK079307).

REFERENCES

Acharya P, Beckel J, Wang E, Ruiz W, Rojas R, Apodaca G (2004). Distribution of the tight junction proteins ZO-1, occludin, and claudin-4, -8, and -12 in bladder epithelium. Am J Physiol 287, F305–F318.

Apodaca G (2004). The uroepithelium: not just a passive barrier. Traffic 5, 1–12.

Balestreire EM, Apodaca G (2007). Apical EGF receptor signaling: regulation of stretch-dependent exocytosis in bladder umbrella cells. Mol Biol Cell 18, 1312–1323.

Barr F, Lambright DG (2010). Rab GEFs and GAPs. Curr Opin Cell Biol 22, 461–470.

Benli M, Doring F, Robinson DG, Yang X, Gallwitz D (1996). Two GTPase isoforms, Ypt31p and Ypt32p, are essential for Golgi function in yeast. EMBO J 15, 6460–6475.

Bond LM, Brandstaetter H, Sellers JR, Kendrick-Jones J, Buss F (2011). Myosin motor proteins are involved in the final stages of the secretory pathways. Biochem Soc Trans 39, 1115–1119.

Born M, Pahner I, Ahnert-Hilger G, Jons T (2003). The maintenance of the permeability barrier of bladder facet cells requires a continuous fusion of discoid vesicles with the apical plasma membrane. Eur J Cell Biol 82, 343–350.

Bossu P *et al*. (2000). A dominant negative RAS-specific guanine nucleotide exchange factor reverses neoplastic phenotype in K-ras transformed mouse fibroblasts. Oncogene 19, 2147–2154.

Brondyk WH, McKiernan CJ, Fortner KA, Stabila P, Holz RW, Macara IG (1995). Interaction cloning of Rabin3, a novel protein that associates with the Ras-like GTPase Rab3A. Mol Cell Biol 15, 1137–1143.

Brunner Y, Coute Y, Iezzi M, Foti M, Fukuda M, Hochstrasser DF, Wollheim CB, Sanchez JC (2007). Proteomics analysis of insulin secretory granules. Mol Cell Proteomics 6, 1007–1017.

Bryant DM, Datta A, Rodriguez-Fraticelli AE, Peränen J, Martin-Belmonte F, Mostov KE (2010). A molecular network for de novo generation of the apical surface and lumen. Nat Cell Biol 12, 1035–1045.

Casanova JE, Wang X, Kumar R, Bhartur SG, Navarre J, Woodrum JE, Altschuler YA, Ray GS, Godenring JR (1999). Association of Rab25 and Rab11a with the apical recycling system of polarized Madin-Darby canine kidney cells. Mol Biol Cell 10, 47–61.

Casey TM, Meade JL, Hewitt EW (2007). Organelle proteomics: identification of the exocytic machinery associated with the natural killer cell secretory lysosome. Mol Cell Proteomics 6, 767–780.

Chen Y, Guo X, Deng F-M, Liang F-X, Sun W, Ren M, Izumi T, Sabatini DD, Sun T-T, Kreibich G (2003). Rab27b is associated with fusiform vesicles and may be involved in targeting uroplakins to urothelial apical membranes. Proc Natl Acad Sci USA 100, 14012–14017.

Chu BB, Ge L, Xie C, Zhao Y, Miao HH, Wang J, Li BL, Song BL (2009). Requirement of myosin Vb-Rab11a-Rab11-FIP2 complex in cholesterol-regulated translocation of NPC1L1 to the cell surface. J Biol Chem 284, 22481–22490.

de Bruijn DR, dos Santos NR, Kater-Baats E, Thijssen J, van den Berk L, Stap J, Balemans M, Schepens M, Merkx G, van Kessel AG (2002). The cancer-related protein SSX2 interacts with the human homologue of a Ras-like GTPase interactor, RAB3IP, and a novel nuclear protein, SSX2IP. Genes Chromosomes Cancer 34, 285–298.

Diekmann Y, Seixas E, Gouw M, Tavares-Cadete F, Seabra MC, Pereira-Leal JB (2011). Thousands of rab GTPases for the cell biologist. PLoS Comput Biol 7, e1002217.

Duman JG, Tyagarajan K, Kolsi MS, Moore HP, Forte JG (1999). Expression of rab11a N124I in gastric parietal cells inhibits stimulatory recruitment of the H+-K+-ATPase. Am J Physiol Cell Physiol 277, C361–C372.

Eitzen G, Will E, Gallwitz D, Haas A, Wickner W (2000). Sequential action of two GTPases to promote vacuole docking and fusion. EMBO J 19, 6713–6720.

Feng S, Knodler A, Ren J, Zhang J, Zhang X, Hong Y, Huang S, Peranen J, Guo W (2012). A Rab8 guanine nucleotide exchange factor-effector interaction network regulates primary ciliogenesis. J Biol Chem 287, 15602–15609.

Fukuda M (2008). Regulation of secretory vesicle traffic by Rab small GTPases. Cell Mol Life Sci 65, 2801–2813.

Fukuda M (2011). TBC proteins: GAPs for mammalian small GTPase Rab. Biosci Rep 31, 159–168.

Grigoriev I *et al*. (2011). Rab6, Rab8, and MICAL3 cooperate in controlling docking and fusion of exocytotic carriers. Curr Biol 21, 967–974.

Guo X *et al*. (2009). Involvement of vps33a in the fusion of uroplakin-degrading multivesicular bodies with lysosomes. Traffic 10, 1350–1361.

Handley MT, Haynes LP, Burgoyne RD (2007). Differential dynamics of Rab3A and Rab27A on secretory granules. J Cell Sci 120, 973–984.

Hattula K, Furuhjelm J, Arffman A, Peranen J (2002). A Rab8-specific GDP/GTP exchange factor is involved in actin remodeling and polarized membrane transport. Mol Biol Cell 13, 3268–3280.

Huber LA, Pimplikar S, Parton RG, Virta H, Zerial M, Simons K (1993). Rab8, a small GTPase involved in vesicular traffic between the TGN and the basolateral plasma membrane. J Cell Biol 123, 35–45.

Hudoklin S, Jezernik K, Neumuller J, Pavelka M, Romih R (2012). Electron tomography of fusiform vesicles and their organization in urothelial cells. PLoS One 7, e32935.
Hudoklin S, Zupancic D, Romih R (2009). Maturation of the Golgi apparatus in urothelial cells. Cell Tissue Res 336, 453–463.
Hutagalung AH, Novick PJ (2011). Role of Rab GTPases in membrane traffic and cell physiology. Physiol Rev 91, 119–149.
Jin Y, Sultana A, Gandhi P, Franklin E, Hamamoto S, Khan AR, Munson M, Schekman R, Weisman LS (2011). Myosin V transports secretory vesicles via a Rab GTPase cascade and interaction with the exocyst complex. Dev Cell 21, 1156–1170.
Kerr DE, Liang F, Bondioli KR, Zhao H, Kreibich G, Wall RJ, Sun TT (1998). The bladder as a bioreactor: urothelium production and secretion of growth hormone into urine. Nat Biotechnol 16, 75–79.
Khandelwal P, Ruiz WG, Apodaca G (2010). Compensatory endocytosis in bladder umbrella cells occurs through an integrin-regulated and RhoA- and dynamin-dependent pathway. EMBO J 29, 1961–1975.
Khandelwal P, Ruiz G, Balestreire-Hawryluk E, Weisz OA, Goldenring JA, Apodaca G (2008). Rab11a-dependent exocytosis of discoidal/fusiform vesicles in bladder umbrella cells. Proc Natl Acad Sci USA 105, 15773–15778.
Khvotchev MV, Ren M, Takamori S, Jahn R, Sudhof TC (2003). Divergent functions of neuronal Rab11b in Ca2+-regulated versus constitutive exocytosis. J Neurosci 23, 10531–10539.
Knodler A, Feng S, Zhang J, Zhang X, Das A, Peranen J, Guo W (2010). Coordination of Rab8 and Rab11 in primary ciliogenesis. Proc Natl Acad Sci USA 107, 6346–6351.
Lapierre LA, Dorn MC, Zimmerman CF, Navarre J, Burnette JO, Goldenring JR (2003). Rab11b resides in a vesicular compartment distinct from Rab11a in parietal cells and other epithelial cells. Exp Cell Res 290, 322–331.
Lapierre LA, Kumar R, Hales CM, Navarre J, Bhartur SG, Burnette JO, Provance DWJr, Mercer JA, Bahler M, Goldenring JR (2001). Myosin Vb is associated with plasma membrane recycling systems. Mol Biol Cell 12, 1843–1857.
Lewis S, de Moura J (1982). Incorporation of cytoplasmic vesicles into apical membrane of mammalian urinary bladder epithelium. Nature 297, 685–688.
Lipatova Z, Tokarev AA, Jin Y, Mulholland J, Weisman LS, Segev N (2008). Direct interaction between a myosin V motor and the Rab GTPases Ypt31/32 is required for polarized secretion. Mol Biol Cell 19, 4177–4187.
Manders EMM, Verbeek FJ, Aten JA (1993). Measurement of co-localization of objects in dual-color confocal images. J Microsc 169, 375–382.
Medkova M, France YE, Coleman J, Novick P (2006). The rab exchange factor Sec2p reversibly associates with the exocyst. Mol Biol Cell 17, 2757–2769.
Morozova N, Liang Y, Tokarev AA, Chen SH, Cox R, Andrejic J, Lipatova Z, Sciorra VA, Emr SD, Segev N (2006). TRAPPII subunits are required for the specificity switch of a Ypt-Rab GEF. Nat Cell Biol 8, 1263–1269.
Nedvetsky PI *et al.* (2007). A role of myosin Vb and Rab11-FIP2 in the aquaporin-2 shuttle. Traffic 8, 110–123.
Ortiz D, Medkova M, Walch-Solimena C, Novick P (2002). Ypt32 recruits the Sec4p guanine nucleotide exchange factor, Sec2p, to secretory vesicles; evidence for a Rab cascade in yeast. J Cell Biol 157, 1005–1015.
Parkhitko CA, Favorova CO, Henske EP (2011). Rabin8 protein interacts with GTPase Rheb and inhibits phosphorylation of Ser235/Ser236 in small ribosomal subunit protein S6. Acta Naturae 3, 71–76.
Park W, Mosteller RD, Broek D (1997). Identification of a dominant-negative mutation in the yeast CDC25 guanine nucleotide exchange factor for Ras. Oncogene 14, 831–836.
Pavlos NJ, Gronborg M, Riedel D, Chua JJ, Boyken J, Kloepper TH, Urlaub H, Rizzoli SO, Jahn R (2010). Quantitative analysis of synaptic vesicle Rabs uncovers distinct yet overlapping roles for Rab3a and Rab27b in Ca2+-triggered exocytosis. J Neurosci 30, 13441–13453.
Pavlos NJ, Jahn R (2011). Distinct yet overlapping roles of Rab GTPases on synaptic vesicles. Small GTPases 2, 77–81.
Poteryaev D, Datta S, Ackema K, Zerial M, Spang A (2010). Identification of the switch in early-to-late endosome transition. Cell 141, 497–508.
Prekeris R, Terrian DM (1997). Brain myosin V is a synaptic vesicle-associated motor protein: evidence for a Ca2+-dependent interaction with the synaptobrevin-synaptophysin complex. J Cell Biol 137, 1589–1601.
Provance DW Jr, Addison EJ, Wood PR, Chen DZ, Silan CM, Mercer JA (2008). Myosin-Vb functions as a dynamic tether for peripheral endocytic compartments during transferrin trafficking. BMC Cell Biol 9, 44.
Rindler MJ, Xu CF, Gumper I, Smith NN, Neubert TA (2007). Proteomic analysis of pancreatic zymogen granules: identification of new granule proteins. J Proteome Res 6, 2978–2992.
Rink J, Ghigo E, Kalaidzidis Y, Zerial M (2005). Rab conversion as a mechanism of progression from early to late endosomes. Cell 122, 735–7489.
Rivera-Molina FE, Novick PJ (2009). A Rab GAP cascade defines the boundary between two Rab GTPases on the secretory pathway. Proc Natl Acad Sci USA 106, 14408–14413.
Roland JT, Bryant DM, Datta A, Itzen A, Mostov KE, Goldenring JR (2011). Rab GTPase-Myo5B complexes control membrane recycling and epithelial polarization. Proc Natl Acad Sci USA 108, 2789–2794.
Roland JT, Kenworthy AK, Peranen J, Caplan S, Goldenring JR (2007). Myosin Vb interacts with Rab8a on a tubular network containing EHD1 and EHD3. Mol Biol Cell 18, 2828–2837.
Romih R, Veranic P, Jezernik K (1999). Actin filaments during terminal differentiation of urothelial cells in the rat urinary bladder. Histochem Cell Biol 112, 375–380.
Rudolf R, Bittins CM, Gerdes HH (2011). The role of myosin V in exocytosis and synaptic plasticity. J Neurochem 116, 177–191.
Schluter OM, Schmitz F, Jahn R, Rosenmund C, Sudhof TC (2004). A complete genetic analysis of neuronal Rab3 function. J Neurosci 24, 6629–6637.
Schuh M (2011). An actin-dependent mechanism for long-range vesicle transport. Nat Cell Biol 13, 1431–1436.
Starr T, Sun Y, Wilkins N, Storrie B (2010). Rab33b and Rab6 are functionally overlapping regulators of Golgi homeostasis and trafficking. Traffic 11, 626–636.
Staudt T, Lang MC, Medda R, Engelhardt J, Hell SW (2007). 2,2′-Thiodiethanol: a new water soluble mounting medium for high resolution optical microscopy. Microsc Res Tech 70, 1–9.
Swiatecka-Urban A *et al.* (2007). Myosin Vb is required for trafficking of the cystic fibrosis transmembrane conductance regulator in Rab11a-specific apical recycling endosomes in polarized human airway epithelial cells. J Biol Chem 282, 23725–23736.
Takamori S *et al.* (2006). Molecular anatomy of a trafficking organelle. Cell 127, 831–846.
Truschel ST, Wang E, Ruiz WG, Leung SM, Rojas R, Lavelle J, Zeidel M, Stoffer D, Apodaca G (2002). Stretch-regulated exocytosis/endocytosis in bladder umbrella cells. Mol Biol Cell 13, 830–846.
Tsuboi T, Fukuda M (2006). Rab3A and Rab27A cooperatively regulate the docking step of dense-core vesicle exocytosis in PC12 cells. J Cell Sci 119, 2196–2203.
Ullrich O, Reinsch S, Urbe S, Zerial M, Parton RG (1996). Rab11 regulates recycling through the pericentriolar recycling endosome. J Cell Biol 135, 913–924.
Varthakavi V, Smith RM, Martin KL, Derdowski A, Lapierre LA, Goldenring JR, Spearman P (2006). The pericentriolar recycling endosome plays a key role in Vpu-mediated enhancement of HIV-1 particle release. Traffic 7, 298–307.
Veranic P, Jezernik K (2002). Trajectorial organisation of cytokeratins within the subapical region of umbrella cells. Cell Motil Cytoskeleton 53, 317–325.
Volpicelli LA, Lah JJ, Fang G, Goldenring JR, Levey AI (2002). Rab11a and myosin Vb regulate recycling of the M4 muscarinic acetylcholine receptor. J Neurosci 22, 9776–9784.
Wakabayashi Y, Dutt P, Lippincott-Schwartz J, Arias IM (2005). Rab11a and myosin Vb are required for bile canalicular formation in WIF-B9 cells. Proc Natl Acad Sci USA 102, 15087–15092.
Wang H, Liang FX, Kong XP (2008). Characteristics of the phagocytic cup induced by uropathogenic *Escherichia coli*. J Histochem Cytochem 56, 597–604.
Wang E, Truschel ST, Apodaca G (2003). Analysis of hydrostatic pressure-induced changes in umbrella cell surface area. Methods 30, 207–217.
Watanabe M *et al.* (2005). Myosin-Va regulates exocytosis through the submicromolar Ca2+-dependent binding of syntaxin-1A. Mol Biol Cell 16, 4519–4530.
Wu XR, Kong XP, Pellicer A, Kreibich G, Sun TT (2009). Uroplakins in urothelial biology, function, and disease. Kidney Int 75, 1153–1165.
Xu S, Edman M, Kothawala MS, Sun G, Chiang L, Mircheff A, Zhu L, Okamoto C, Hamm-Alvarez S (2011). A Rab11a-enriched subapical membrane compartment regulates a cytoskeleton-dependent transcytotic pathway in secretory epithelial cells of the lacrimal gland. J Cell Sci 124, 3503–3514.
Yu W, Khandelwal P, Apodaca G (2009). Distinct apical and basolateral membrane requirements for stretch-induced membrane traffic at the apical surface of bladder umbrella cells. Mol Biol Cell 20, 282–295.
Zhu H, Liang Z, Li G (2009). Rabex-5 is a Rab22 effector and mediates a Rab22-Rab5 signaling cascade in endocytosis. Mol Biol Cell 20, 4720–4729.